

## ESTIMATION OF URBAN SPRAWL AND VEGETATION LOSS OF METRO CEBU THROUGH MULTI-TEMPORAL IMAGE ANALYSIS

Chito Patiño (1), Florencio Campomanes V (1), Mary Joyce Flores (1,2)

<sup>1</sup> Central Visayas Center for Environmental Informatics, University of the Philippines Cebu, Lahug, Cebu City, 6000, Philippines

<sup>2</sup> Department of Biology and Environmental Science, College of Science, University of the Philippines Cebu, Lahug, Cebu City, 6000, Philippines

Email: [clpatino@up.edu.ph](mailto:clpatino@up.edu.ph); [fpcampomanes@up.edu.ph](mailto:fpcampomanes@up.edu.ph); [mlflores2@up.edu.ph](mailto:mlflores2@up.edu.ph)

**KEY WORDS:** ndvi, urban growth, remote sensing

**ABSTRACT:** The rapid urbanization in Cebu in recent years changed the land use patterns in the province. Areas allotted to forest or agricultural use are on a decline. In order to gain insight to the extent of vegetation loss in relation to the expanding urban sprawl in Cebu, multi-temporal analysis of Landsat images covering Cebu City, Mandaue City, Consolacion, Liloan, Lapu-Lapu City (excluding Olango island), and Cordova for the period 1994 to 2019 was conducted. The NDVI, NDMI, and Tasseled Cap (TC) indices were computed to aid in the Land Use/Land Cover classification of the different Landsat images. After classification, urban density, growth rate, and vegetation loss were estimated. Urbanization was found to have widened in all the of the study areas but at different paces. Notable for their growth rates are Mandaue City and Lapu-Lapu City. Lapu-Lapu have four of the “fastest” growing grids while Mandaue have the 5<sup>th</sup> fastest growing grid. The direction of urbanization since 1994 was also determined. The identification of areas of rapid growth and considerable vegetation loss provide government officials basis for land use regulation. Enactment of updated land use plans by local governments is recommended to ensure the rational allocation and proper use of limited land resources.

### 1. INTRODUCTION

The rapid urbanization in Cebu in recent years changed the land use patterns in the province. Metro Cebu is considered the second biggest urban center in the Philippines. The rise of new residential subdivisions, commercial zones, and industrial complexes have led widespread yet unquantified vegetation loss. Urbanization has encroached into agricultural and forest lands. Vegetation loss impairs the capacity of nature to provide ecosystem services vital to the population’s well-being such as reduction of air quality, reduction of air pollution, and climate regulation (De Carvalho & Szlafsztein, 2019).

Remote sensing and GIS techniques have been used to detect changes in land use, forest disturbances, and/or land degradation particularly utilizing Landsat multitemporal images (Amine & Hadria, 2012; Boori, Netzband, Choudhary, & Voženílek, 2015; Devries, Pratihast, Verbesselt, Kooistra, & Herold, 2016; Hislop et al., 2018; Plaiklang et al., 2008; Schultz et al., 2016). Meanwhile, identifying current land use/land cover through classification of Landsat images has been extensively utilized in several researches and contexts (Ali & Salman, 2016; Amine & Hadria, 2012; Boori et al., 2015; Devries et al., 2016; Rokni, Ahmad, Selamat, & Hazini, 2014; Schultz et al., 2016; Vorovencii, 2007; Wilson & Sader, 2002; Young et al., 2017). These techniques can be utilized to satisfy our objectives to wit: (1) identify and measure past and present land cover, (2) estimate vegetation loss, and (3) determine past and present urban density, and, lastly, calculate the urban growth rates of the cities of Cebu, Mandaue, and Lapu-Lapu (excluding Olango Island), as well as the municipalities of Consolacion, Cordova, and Liloan.

### 2. MATERIALS AND METHODS

#### 2.1 Study Area and Data

The study covers the cities of Cebu, Mandaue, and Lapu-Lapu (excluding Olango Island), as well as the municipalities of Consolacion, Cordova, and Liloan. Three Landsat images with the less than 20% cloud cover from different decades were downloaded. A temporal difference spanning at least 10 years between images was targeted to see significant land use or land cover change. However, due to limited availability of data with little to no cloud cover, data from the years 1994, 2002, and 2019 were the ones acquired. Specifically, a Landsat 5 TM from 1994 (USGS, 1994), Landsat 7 ETM+ from 2002 (USGS, 2002), and Landsat 8 OLI from 2019 (USGS, 2019) which were preprocessed from digital numbers (DN) to surface reflectance (SR) using the Landsat Ecosystem Disturbance

Adaptive Processing System (LEDAPS) for Landsat 5 TM and Landsat 7 ETM+ images and the Landsat Surface Reflectance Code (LaSRC) for Landsat 8 OLI image (See Fig. 1-3).



Figure 1. RGB Composite of study area, 1994. Landsat images courtesy of the U.S. Geological Survey

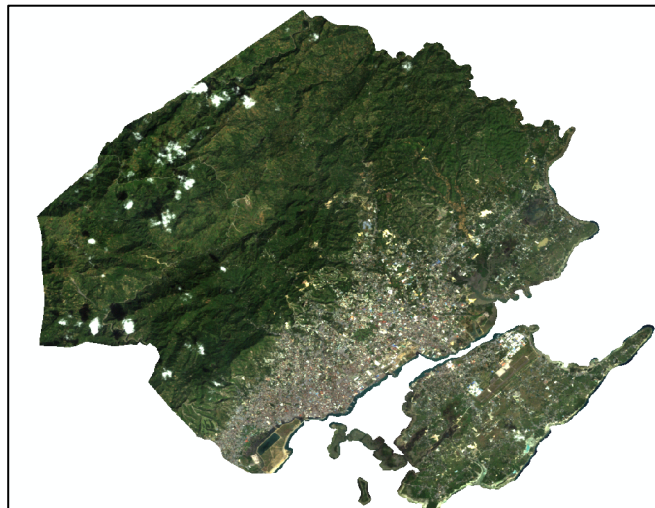


Figure 2. RGB Composite of study area, 2002. Landsat images courtesy of the U.S. Geological Survey

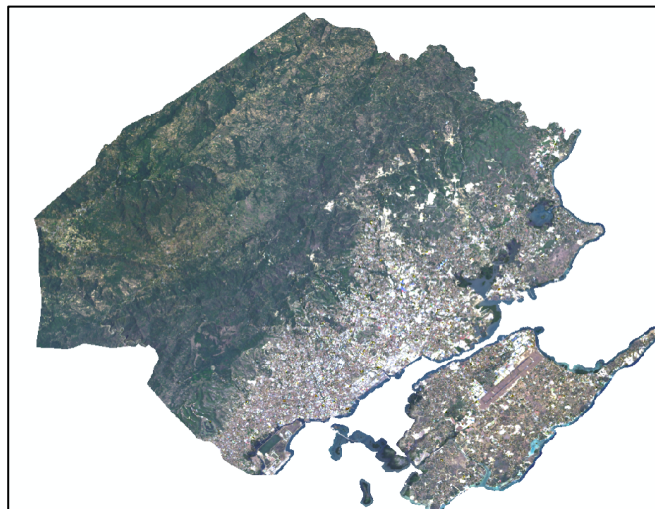


Figure 3. RGB Composite of study area, 2019. Landsat images courtesy of the U.S. Geological Survey

Table 1 displays the relevant information about each image collected.

Table 1. Metadata of Landsat images used in the study

Sensor	Date	Spatial Resolution	Bands used (RGB, NIR, SWIR)
Landsat 5 TM	July 21, 1994	30m	1-5, 7
Landsat 7 ETM	December 26, 2002	30m	1-5, 7
Landsat 8 OLI	April 21, 2019	30m	2-7

## 2.2 Methods

The general method for the Land Use/Land Cover classification is shown in the flow chart below (Fig. 4) with the major components discussed in the succeeding sections.

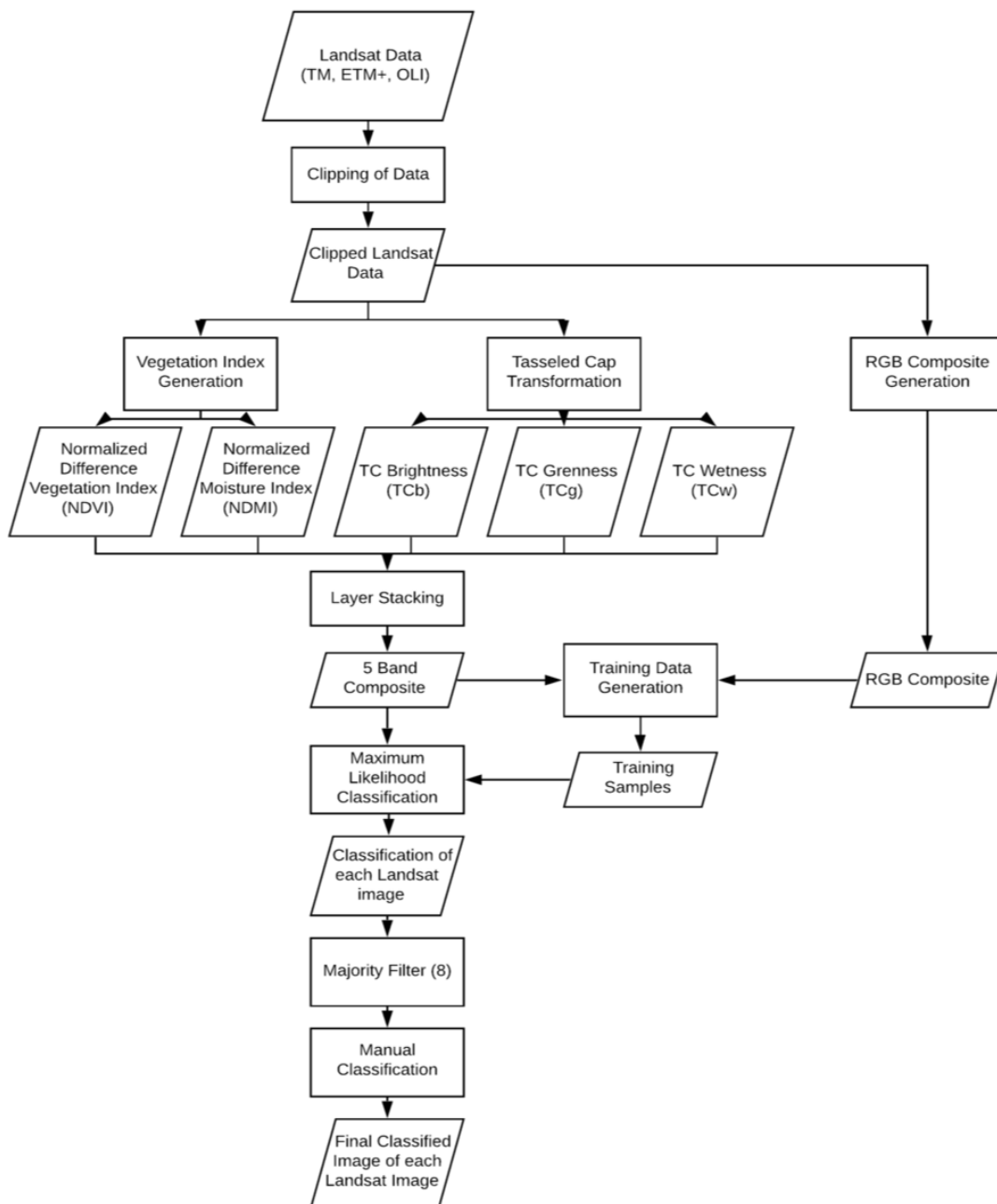


Figure 4. Flow chart of land use/land cover classification

### 2.2.1 Image Preprocessing and Vegetation Indices

After the collection and preprocessing of Landsat images, vegetation indices (VIs) are computed to aid in the classification of these images. Landsat preprocessing methods are adopted as discussed by Young et al. (2017). From the surface reflectance, Normalized Difference Vegetation Index (NDVI) and Normalized Difference Moisture Index (NDMI) were calculated for each image. NDVI is used to quantify increase or decrease of vegetation greenness while NDMI is used to quantify vegetation water content (Wilson & Sader, 2002). Both were calculated using Eq. (1) and (2), respectively:

$$NDVI = \frac{(NIR - R)}{(NIR + R)} \quad (1)$$

$$NDMI = \frac{(NIR - SWIR)}{(NIR + SWIR)} \quad (2)$$

### 2.2.2 Tasseled Cap Transformation (TCT)

The VIs above are only limited to the use of the NIR, SWIR, and R band. We proceed with Tasseled Cap Transformation to utilize the rest of the available bands i.e. G and B (Ali & Salman, 2016; Amine & Hadria, 2012; Schultz et al., 2016; Vorovencii, 2007). The different bands of TCT (Brightness (TCb), Greenness (TCg), and Wetness (TCw)) are calculated from the surface reflectance images from all years using the following equations (Eq. 3, 4, and 5):

$$TCb = b_1B + b_2R + b_3G + b_4NIR + b_5SWIR1 + b_6SWIR2 \quad (3)$$

$$TCg = g_1B + g_2R + g_3G + g_4NIR + g_5SWIR1 + g_6SWIR2 \quad (4)$$

$$TCw = w_1B + w_2R + w_3G + w_4NIR + w_5SWIR1 + w_6SWIR2 \quad (5)$$

where each coefficient is defined in Table 2 for each band.

Table 2. Tasseled Cap Coefficients for surface reflectance data

	B	G	R	NIR	SWIR1	SWIR2
TCb (b)	0.2043	0.4158	0.5524	0.5741	0.3124	0.2303
TCg (g)	-0.1603	0.2819	-0.4934	0.7940	-0.0002	-0.1446
TCw (w)	0.0315	0.2021	0.3102	0.1594	-0.6806	-0.6109

### 2.2.3 Layer Stacking

The resulting vegetation and Tasseled Cap (TC) indices were stacked to create one 5-band composite image for each year where the TC indices were the first three bands (b,g,w), followed by the NDVI (Band 4) and lastly, the NDMI (Band 5). Each composite image will be used in both the creation of training samples as well as the maximum likelihood classification process.

### 2.2.4 Classification

Since the study is focused on urban sprawl, the number of classes for the classification process were limited to four, namely, "Water", "Urban", "Undeveloped/Bare", and "Vegetation". These four main classes are described in detail in Table 3.

Table 3. Description of land use/classes used

Land Use/Class	Description
Water	Water bodies, coast, rivers, lakes, open sea
Urban	Residential, commercial, industrial, roads, mixed urban
Undeveloped/Bare	Dry soil, mining areas, dry agricultural land, very sparse vegetation

Classification will be processed using the Image Classification toolbar in ArcMap 10.6 following a tutorial by Nagi (2011). Training samples were collected for each year by digitizing accurate polygons of each class. Scatterplots for each year were created and examined to check the separability of each class at each band combination. When the separability of all training samples were satisfactory, training signature files were created to be used in the Maximum Likelihood (ML) classification with equal a priori probability weighting. To reduce the “salt and pepper” effect of the resulting classification, a majority filter using eight neighbors was used. Minor clouds and haze found near the mountainous areas were manually classified and presumed as vegetation since these were found in forested areas.

### 2.2.5 Urban Density and Annual Urban Growth Rate Calculation

For this study, we utilize the process outlined by Boori et al., (2015) that introduces multi-buffer rings in calculating for urban density and growth rate and the subsequent visualization. The methodology of urban density and urban growth rate calculation is seen in the flow chart below (Fig. 5):

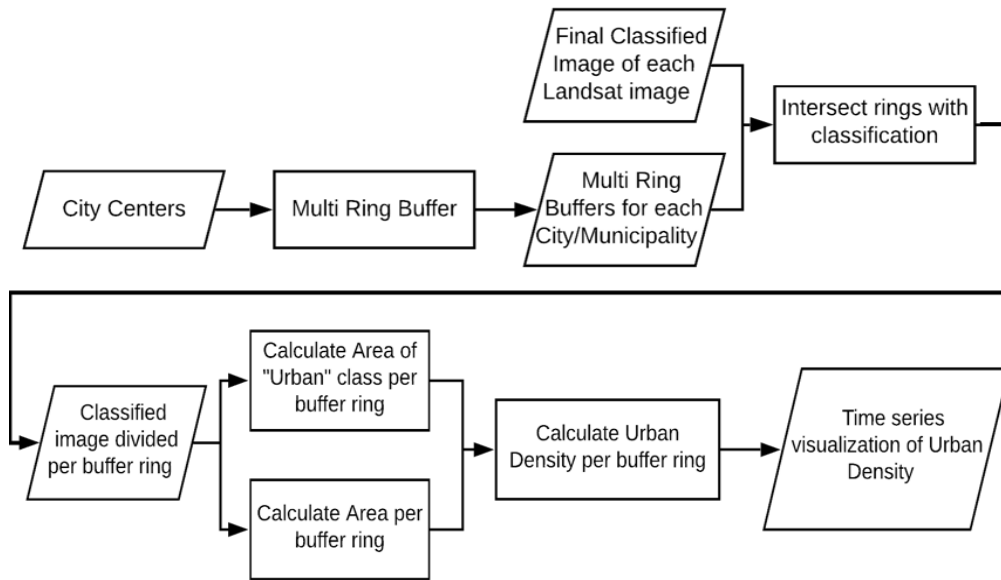


Figure 5. Process flow for urban density and urban growth rate calculation

To calculate urban density, multi-buffer rings were created for every 1 kilometer from the city center up to 10 kilometers then every 5 kilometers succeeding that. Since the cities and municipalities included in this study do not have a well defined “city center”, their respective municipal or city halls were used as their city centers. These rings were then intersected with the final classification output per municipality for all three years. The area per class per ring for all three years were calculated as well as the total urban area for each year. Urban density of each ring was derived using the following equation:

$$UrbanDensity_{ring} = \frac{Area\ of\ Urban\ class_{ring}}{Total\ area_{ring}} \quad (6)$$

The urban densities of each city/municipality are then visualized to see the difference over time.

To calculate the magnitude of the urbanization per unit area, an indicator called annual urban growth rate was adapted:

$$AnnualUrbanGrowthRate = \frac{(Area\ of\ Urban\ class_{recent\ year} - Area\ of\ Urban\ class_{earliest\ year})}{Recent\ Year - Earliest\ Year} \quad (7)$$

The whole study area was divided into 1 km grids for uniformity and the area of the “Urban” class for the most recent year and the earliest year was calculated for each grid. In this study, the difference of the 2019 result and the 1994 result was calculated. The difference in urban area was then divided by the number of years between the images to

get the annual urban growth rate. The annual urban growth rate of each municipality/city was also calculated using the same formula.

### 3. RESULTS AND DISCUSSION

#### 3.1 Classification

The NDVI, NDMI, and Tasseled Cap (TC) indices were created to aid in the Land Use/Land Cover classification of the different Landsat images. Fig. 6 shows the resulting maps of Tasseled Cap Indices Composite for the years 1994, 2002, and 2019.

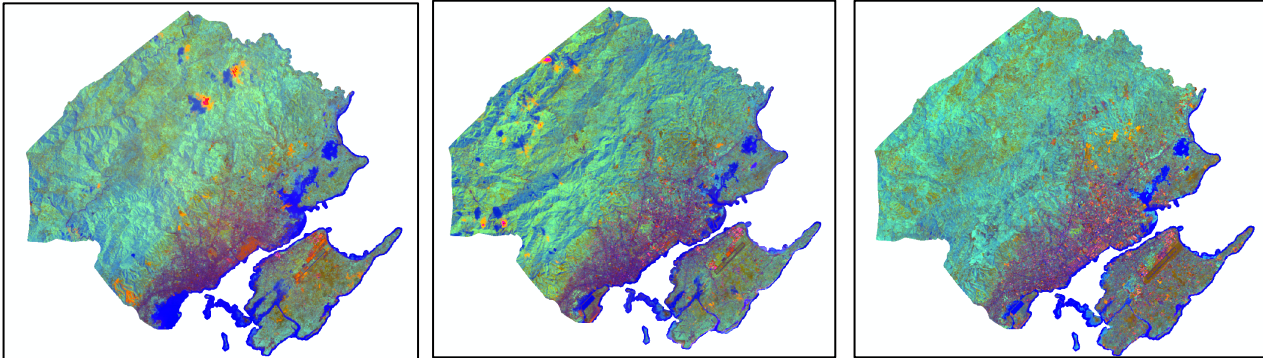


Figure 6. (L-R) Tasseled Cap Indices Composite from 1994, 2002, and 2019.

The Landsat maps used in this study had cloud cover (<20%). In the TC composite, shadows caused by cloud cover show the same characteristics as water. However, this issue is addressed by manually classifying the clouds.

Scatterplots were created after training sample collection to examine the separability of the collected training samples (See Fig. 7-9).

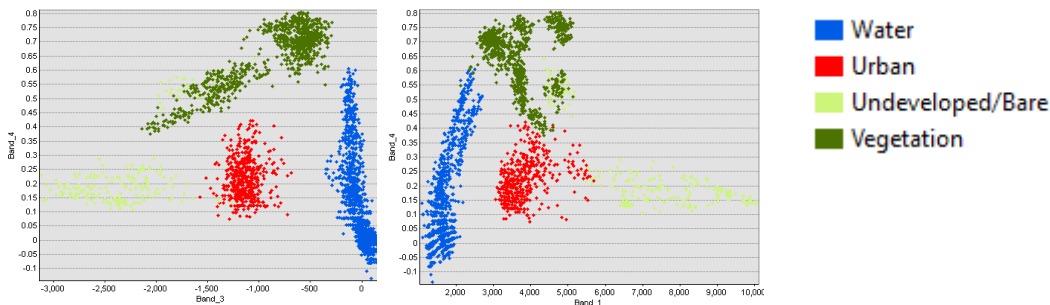


Figure 7. Scatterplots of the training samples for 1994 images. (L) NDVI vs. TCb, (R) NDVI vs. TCw

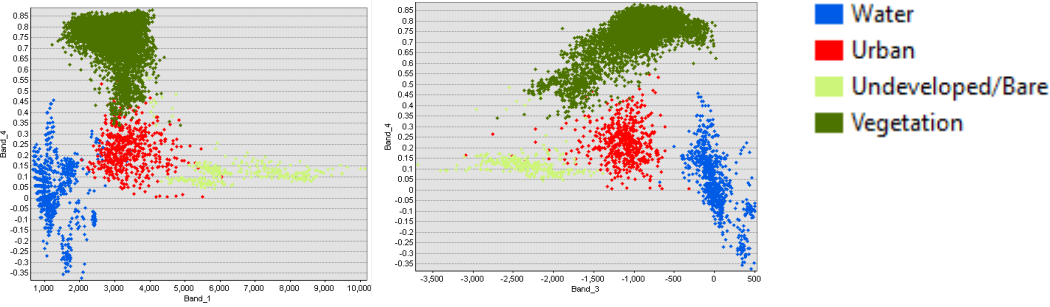


Figure 8. Scatterplots of the training samples for 2002 images. (L) NDVI vs. TCb, (R) NDVI vs. TCw

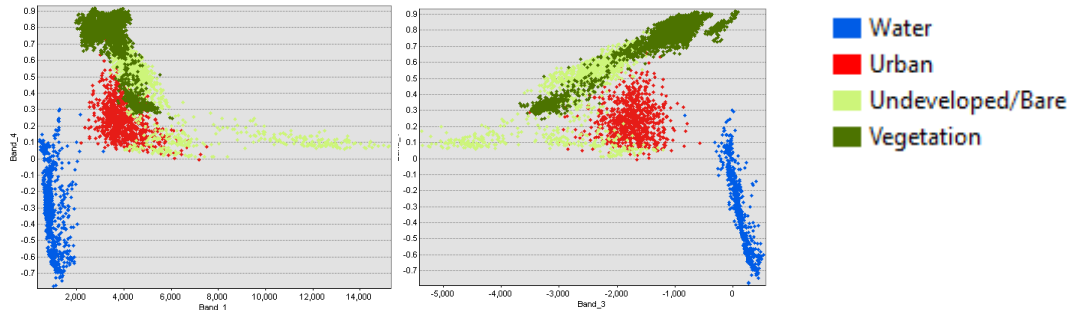


Figure 9. Scatterplots of the training samples for 2019 images. (L) NDVI vs. TCb, (R) NDVI vs. TCw

For all three study years, three inputs showed potential in separating the classes, namely, NDVI, TCb, and TCw. The NDVI vs. TCb and NDVI vs. TCw scatterplots showed to have the most separability among classes. It can also be observed that the separability between urban and undeveloped/bare training samples are not so evident for the 2019 image training samples. This could be caused by the increase of subdivision development hence, urban areas mixed with dry land/soil.

The classification result for each study year is shown in Fig. 10. It can be observed that the 2019 result is quite different from the 1994 and 2002 result with respect to the undeveloped/bare class in the northern part of the study area. This is caused by the drying of land due to summer. As this was the most recent cloudless image available, and considering that the focus of this section would be on the urban class, this was not going to affect the study significantly.

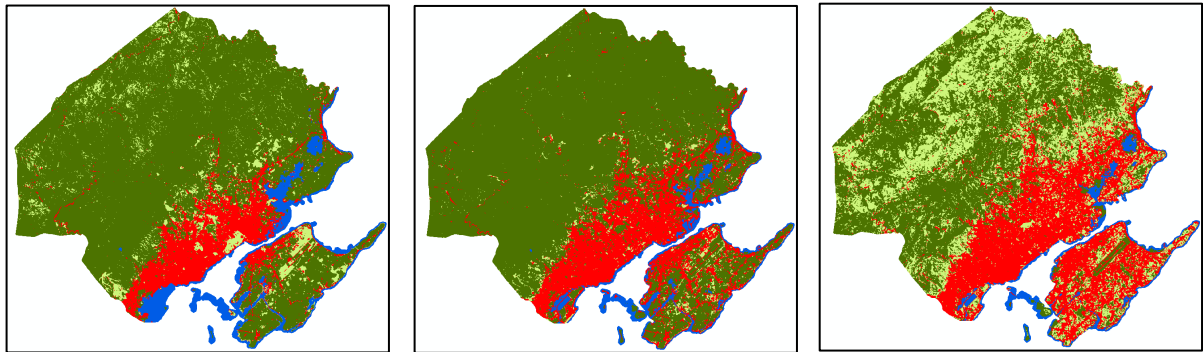


Figure 10. (L-R) Maximum Likelihood Classification outputs for 1994, 2002, 2019.

### 3.2 Urban Density

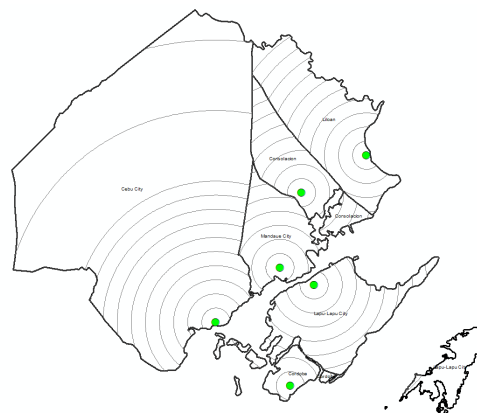


Figure 11. Multi-ring buffer zones for each city/municipality including their centers

Given that the municipalities and cities included in the study are quite small with the exception of Cebu City, it can be seen that most of the multi-ring buffers do not go farther than 10 km (See Fig. 11). The urban density for each ring were calculated for each study year and visualized.

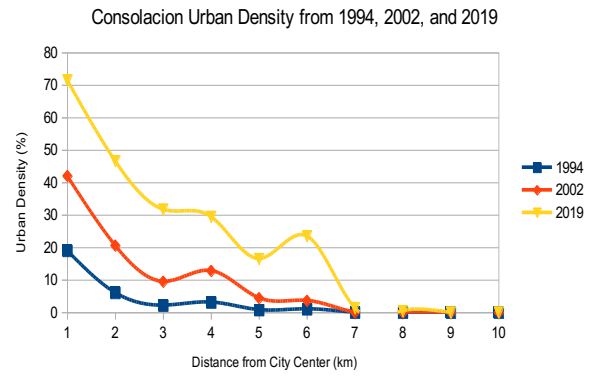
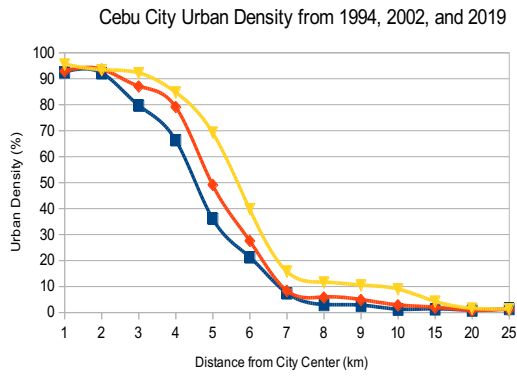


Figure 12. (L-R) Urban density of Cebu City and Consolacion from center outward for 1994, 2002, and 2019.

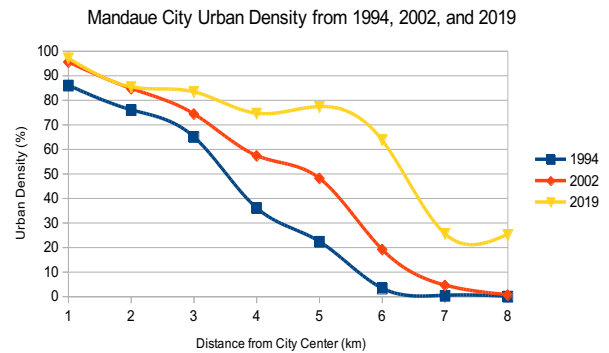
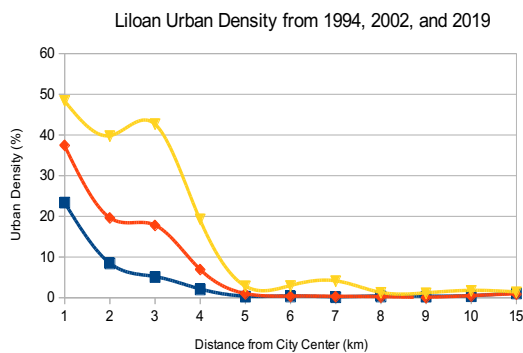


Figure 13. (L-R) Urban density of Cordova and Lapu-Lapu City from center outward for 1994, 2002, and 2019.

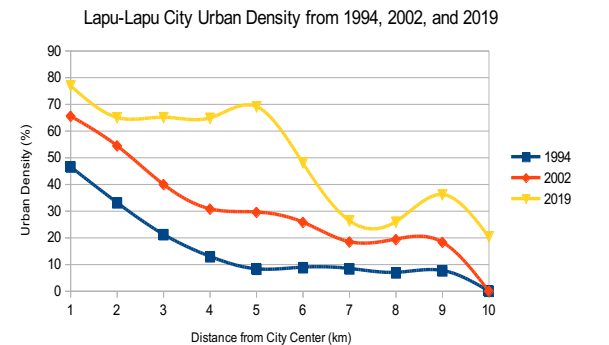
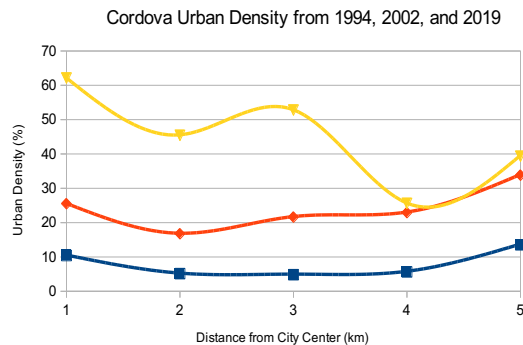


Figure 14. (L-R) Urban density of Liloan and Mandaue City from center outward for 1994, 2002, and 2019.

As seen in Fig. 12 to 14, the urban densities at the 1 km ring buffers for non-cities (Cordova, Liloan, Consolacion) during 1994 were all less than 30% but increasing, even in 2019. At the 1 km ring, Cebu City and Mandaue City both had urban densities above 80% in 1994 with only minor growth in 2002 and 2019. However, the bulk of their urban growth is found between the 3 and 7 km ring buffers with the largest increase being approx. 60% for Mandaue City at the 6 km ring and approx. 30% for Cebu City at the 5 km ring. Cebu City still has noticeable increases even up to the 10 km buffer. Lapu-Lapu City started with only less than 50% urban density in 1994 but accrued almost 80% in 2019. It can also be observed that Lapu-Lapu maintains approx. 60% urban density until the 5 km ring. For all 6 study areas, it is also evident that the urban density decreases as distance from the center increases which shows that urban areas are still concentrated in the city/municipality centers and only few areas far from the center are urbanized.

### 3.3 Annual Growth Rate and Vegetation Loss

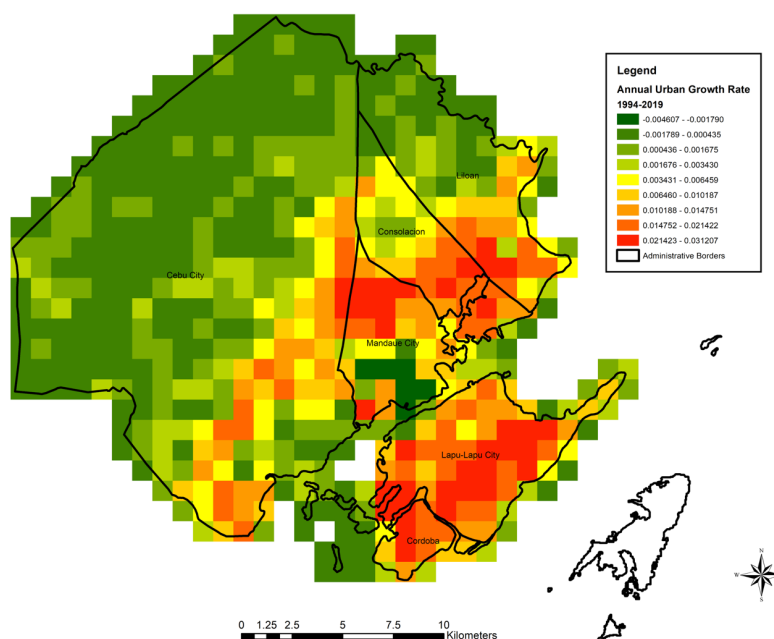


Figure 11. Annual Urban Growth Rate of entire study area

With the resulting AGR result, it can be seen that the entire study area has increased in terms of urbanization but at different paces. The two most evident in terms of urban growth are Mandaue City and Lapu-Lapu City with 4 of the “fastest” growing grids belonging to Lapu-Lapu City and the 5<sup>th</sup> fastest growing grid belonging to Mandaue City. The fastest annual urban growth rate is at 0.031207 sq. km per year. The result shows the direction of urbanization since 1994. It also shows that Cebu City’s urban growth is more spread out given its large area compared to its neighbors like Mandaue City, Consolacion, Cordova, and Lapu-Lapu City that have relatively smaller land areas. This explains why Cebu City has more yellow and orange grids than red ones.

The overall AGR for each study area was also calculated and is shown in the table below:

Table 4. Urban Area Increase and Annual Urban Growth Rate

	Urban Area Increase (sq. km)			Annual Urban Growth Rate (sq. km/year)		
	1994-2002	2002-2019	1994-2019	1994-2002	2002-2019	1994-2019
<b>Cebu City</b>	6.20	11.57	17.77	0.7746	0.6807	0.7108
<b>Mandaue City</b>	4.38	4.09	8.47	0.5480	0.2404	0.3389
<b>Lapu-Lapu City</b>	9.16	12.53	21.69	1.1450	0.7369	0.8675
<b>Consolacion</b>	3.00	6.24	9.24	0.3748	0.3669	0.3694
<b>Liloan</b>	2.69	5.56	8.25	0.3365	0.3271	0.3301
<b>Cordova</b>	1.34	2.79	4.14	0.1680	0.1643	0.1655

It can be observed that Lapu-Lapu City has the highest AGR with 0.8675 sq. km/year followed by Cebu City at 0.7108 sq. km/year. Mandaue City, Consolacion, and Liloan having similar AGR at around 0.33-0.36 sq. km/year. However, given that Mandaue City has a significantly smaller area compared to Liloan and Consolacion, this AGR has a greater impact to Mandaue City. Moreover, because of Cordova’s small land area, it’s AGR of 0.1655 still has a significant impact. The rates of vegetation loss are found to be: Cebu City at 3.21 sq. km./year, Mandaue City 0.33 sq. km./year, and Lapu-Lapu City 0.91 sq. km./year. Meanwhile, Consolacion, Cordova, and Liloan are experiencing vegetation loss at 0.63 sq. km./year, 0.21 sq. km./year, 0.91 sq. km./year, respectively.

### 4. CONCLUSION

Remote sensing and GIS techniques and the availability of free Landsat images allow the fast computation and monitoring which can keep pace with rapid urban growth. The identification of areas of rapid growth and considerable vegetation loss provide vital information to government efforts in land use regulation. Enactment of updated land use plans by local governments is recommended to arrest vegetation loss and ensure the rational allocation and proper use of limited land resources.

## 5. ACKNOWLEDGEMENT

This research is conducted by the University of the Philippines Cebu Center for Environmental Informatics. We are grateful for the support of the Department of Science and Technology (DOST) and its Niche Centers in the Regions for R&D (NICER) Program.

## 6. REFERENCES

### References from Journals:

- Ali, S. M., & Salman, S. S., 2016. New Tasseled Cap Classification Technique using Landsat-8 OLI Image Bands. *Iraqi Journal of Science*, 57(September), 1612–1619.
- Amine, R., & Hadria, F., 2012. Integration of NDVI indices from the tasseled CAP transformation for change detection in satellite images. *International Journal of Computer Science*, 9(2), 1694–0814.
- Boori, M. S., Netzband, M., Choudhary, K., & Voženilek, V., 2015. Monitoring and modeling of urban sprawl through remote sensing and GIS in Kuala Lumpur, Malaysia. *Ecological Processes*, 4(1), 1–10. <https://doi.org/10.1186/s13717-015-0040-2>
- De Carvalho, R. M., & Szlafsztein, C. F., 2019. Urban vegetation loss and ecosystem services: The influence on climate regulation and noise and air pollution. *Environmental Pollution*, 844–852. <https://doi.org/10.1016/j.envpol.2018.10.114>
- Devries, B., Pratihast, A. K., Verbesselt, J., Kooistra, L., & Herold, M., 2016. Characterizing forest change using community-based monitoring data and landsat time series. *PLoS ONE*, 11(3), 1–25. <https://doi.org/10.1371/journal.pone.0147121>
- Hislop, S., Jones, S., Soto-Berelov, M., Skidmore, A., Haywood, A., & Nguyen, T. H., 2018. Using landsat spectral indices in time-series to assess wildfire disturbance and recovery. *Remote Sensing*, 10(3), 1–17. <https://doi.org/10.3390/rs10030460>
- Plaiklang, S., Ongsomwang, S., Prayoonpokarach, S., Horkaew, P., Puttinaovarat, S., Sutthivanich, I., ... Thongrueng, N., 2008. *Using the Geoinformatics Technology for Soil Degradation Assessment in Upper Lamchiengkrai Watershed*, . (1).
- Rokni, K., Ahmad, A., Selamat, A., & Hazini, S., 2014. Water feature extraction and change detection using multitemporal landsat imagery. *Remote Sensing*, 6(5), 4173–4189. <https://doi.org/10.3390/rs6054173>
- Schultz, M., Clevers, J. G. P. W., Carter, S., Verbesselt, J., Avitabile, V., Quang, H. V., & Herold, M., 2016. Performance of vegetation indices from Landsat time series in deforestation monitoring. *International Journal of Applied Earth Observation and Geoinformation*, 52(October 2017), 318–327. <https://doi.org/10.1016/j.jag.2016.06.020>
- Vorovencii, I., 2007. Use of the “ Tasseled Cap ” Transformation for the Interpretation of Satellite Images. *Cadastre Journal*, 07(January 2007), 75–82.
- Wilson, E. H., & Sader, S. A., 2002. Detection of Forest Harvest Type Using Multiple Dates of Landsat TM Imagery. *Remote Sensing of Environment*, 80, 385.
- Young, N. E., Anderson, R. S., Chignell, S. M., Vorster, A. G., Lawrence, R., & Evangelista, P. H., 2017. A survival guide to Landsat preprocessing. *Ecology*, 98(4), 920–932. <https://doi.org/10.1002/ecy.1730>

### References from websites:

- Nagi, J., 2011, Classifying Landsat Image Services to Make a Land Cover Map, Retrieved June 2, 2019, from <https://www.esri.com/arcgis-blog/products/product/imagery/classifying-landsat-image-services-to-make-a-land-cover-map/>.
- United States Geological Survey (USGS), Department of the Interior, 1994. LANDSAT-5 TM. Scene ID: LT51130531994202CLT00. (July 21, 1994). Reston, VA. Retrieved June 5, 2019, from USGS Explorer <http://earthexplorer.usgs.gov>.
- USGS, Department of the Interior, 2002. LANDSAT-7 ETM+. Scene ID: LE71130532002360EDC00. (December 26, 2002). Reston, VA. Retrieved June 5, 2019, from USGS Explorer <http://earthexplorer.usgs.gov>.
- USGS, Department of the Interior, 2019. LANDSAT-8 OLI. Scene ID: LC81130532019111LGN00. (April 4, 2019). Reston, VA. Retrieved June 7, 2019, from USGS Explorer <http://earthexplorer.usgs.gov>.